Qualification of the numerical simulation of a Hypothetical Core Disruptive Accident on the MARA 10 test-facility

Marie-France Robbe, Yves Cariou, Eloi Treille, Michel Lepareux

Qualification of the numerical simulation of a Hypothetical Core Disruptive Accident on the MARA10 test-facility

M.F. Robbe[α], **Y. Cariou**[β], **E. Treille**[ξ], **M. Lepareux**[δ]

α CEA Saclay, DRN-DMT-SEMT, 91191 Gif sur Yvette cedex, France
Tel: (33) 1 69 08 87 49, Fax: (33) 1 69 08 52 42, E-mail: mfrobbe@cea.fr
β Novatome, NVPM, 10 rue Juliette Récamier, 69006 Lyon, France
ξ Socotec Industrie, 1 av. du Parc, 78180 Montigny le Bretonneux, France
δ CEA Saclay, DRN-DMT-SEMT, 91191 Gif sur Yvette cedex, France

Abstract

In case of a Hypothetical Core Disruptive Accident (HCDA) in a Liquid Metal Reactor, the interaction between fuel and liquid sodium creates a high pressure gas bubble in the core. The violent expansion of this bubble loads the vessel and the internal structures, whose deformation is important. The experimental test MARA10 simulates a HCDA in a mock-up schematizing simply the reactor block of a Fast Breeder Reactor. The test-facility includes the main internal structures of a Fast Breeder Reactor block: core support structure, diagrid, radial shield and a simple representation of the above core structures. The test-facility is filled with water topped by an air blanket and the explosion is triggered by an explosive charge.

After a description of the MARA10 test-facility and of its modeling, this paper presents an analysis of the computed results and a comparison of the current computed results are compared with the experimental ones and with other numerical results computed previously by the codes SIRIUS and CASTEM-PLEXUS.

Keywords

Core Disruptive Accident, nuclear reactor, explosion, fluid-structure coupling

1. Introduction

In case of a Hypothetical Core Disruptive Accident (HCDA) in a Liquid Metal Reactor, the interaction between fuel and liquid sodium creates a high pressure gas bubble in the core. The violent expansion of this bubble loads the vessel and the internal structures, whose deformation is important.

During the 70s and 80s, the LMFBR integrity was studied with several computer codes validated on experimental data. Those experimental programmes were undertaken by several countries and consisted generally in simplified small-scale test-facilities representing reactors: APRICOT [1] FTR and CBR detail scale models [2], STROVA [3], COVA [4] [5] [6] [7] [8], WINCON [9] and MARA.

Based on a 1/30 scale model of the Superphenix reactor, the French programme MARA involved ten tests of gradual complexity due to the addition of internal deformable structures:
- MARA 1 and 2 considered a vessel partially filled with water and closed by a rigid roof [10],
- MARA 4 represented the main core support structures [11],
- MARA 8 and 9 were closed by a flexible roof [12],
- MARA 10 included the core support structures (CSS) and a simplified representation of the above core structure (ACS) [13].

The MARS test [14] rested on a 1/20 scale mock-up including all the significant internal components.

A lot of computer codes were used in the world to simulate HCDA. For instance, in the United States, not less than seven codes were available: PISCES 2 DELK [15], REXCO [16], MICE, ICECO, ICEPEL, STRAW and SADCAT [17].

In Europe, several 2D axisymmetric computer codes were used. They were progressively improved in order to be able to perform more realistic HCDA simulations. First, the finite difference SURBOUM code [18], from Belgonucléaire and AWRE-Aldermaston, was capable to model uncompressible fluid and thin shells. It was replaced by the finite difference SEURBNUK code [19] developed by JRC-Ispra and AWRE-Aldermaston, which could model compressible fluids. As the fluid-structure coupling adopted in this code was very simple (separate resolution of the fluid and structure motions), the code was finally coupled to the finite element EURDYN code for the structure calculation [20] [21]. The lagrangian finite difference ASTARTE code [22], developed by the ENEA, could compute compressible fluids and thin shells of simple geometry.

In France, two 2D axisymmetric computer codes specialised in HCDA computations were developed by the CEA-Cadarache. The CASSIOPEE code [23] modeled uncompressible fluids with an eulerian description and thin shells with a lagrangian description. It used a weak coupling and rezonings based on the ALE method.

The lagrangian SIRIUS code [24] described fluids and thick structures with the finite difference method and thin structures with the finite element method. The fluid-structure coupling was realised by a slide-line technique and rezonings were performed during calculation because the internal structure presence caused high distortion of the fluid meshes. The SIRIUS code [25] [10] was validated on the MARA programme [26] [27].

At the end of the 80s, it was preferred to add a specific HCDA sodium-bubble-argon tri-component constitutive law [28] to the general ALE fast dynamics finite element CASTEM-PLEXUS code. The HCDA constitutive law was qualified [29] on the CONT benchmark [30].

In order to demonstrate the CASTEM-PLEXUS capability to predict the behaviour of real reactors [31] [32], axisymmetric computations of the MARA series were confronted with the experimental results. The computations performed at the beginning of the 90s showed a rather good agreement between the experimental and computed results for the MARA 8 and MARA 10 tests even if there were some discrepancies which might be eliminated by increasing the fineness of the mesh [33]. On the contrary, the prediction of the MARS structure displacements and strains was overestimated [34].

As the method used for dealing with the fluid-structure coupling was improved since then, it was undertaken another comparison between the experimental and numerical results and a more detailed analysis of the results. After a brief presentation of the MARA 10 test-facility, this paper is focused on the numerical model, the analysis of the results computed by the code CASTEM-PLEXUS and a comparison with the experimental results and previous numerical results computed by SIRIUS and CASTEM-PLEXUS.

2. Description of the MARA10 test-facility

The primary circuit of the Superphenix reactor (Fig. 1) is a "pool" design [35]. The whole core, primary pumps and intermediate heat exchangers are enclosed in the main reactor vessel which is made of stainless steel and welded to the roof slab. The main reactor vessel is encased in a safety vessel also made of stainless steel.

The MARA10 experiment belongs to the MARA test programme defined and realised at the CEA-Cadarache in order to simulate a HCDA in small scale (1/30) mock-ups of the Superphenix reactor block. The external dimensions of the MARA10 test are 55 cm high and 35 cm of radius.

The characteristics of the mock-up are [33]:
- a scale factor of 1/30 for all dimensions and thickness,
- an axisymmetric geometry,
- sodium is represented by water, argon by air and the bubble expansion by an explosive source.

All tests of the MARA series were fired using a 45 g low density low pressure explosive charge of L54/16 composition [36] leading at least to a 1000 MJ full scale energy release [26]. The bare vessels were filled with water leaving a 4.3 cm air gap below the roof [12]. All the vessels were identical and made of 316 steel of 1.2 mm thickness, except between the junctions with the core support plate and the internal heat exchangers where the thickness was locally reduced from 0.9 to 1.1 mm in order to simulate a pinned attachment with the core support structure.

In MARA10, a flexible roof of 10 mm thickness A42 steel was clamped to the roof support [12]. The vessel was welded to a flange bolted to the roof support. The MARA10 test-facility (Fig. 2) included the main internal structures [13] of the Superphenix reactor:
- The core support structure (CSS) was machined from a single block of Au4g aluminium. It was supported by a thin collar attached to the vessel base.
- The diagrid was a 304L steel plate of 8.8 mm thickness just resting under gravity on the inner flange of the core support.
- The radial shield was represented by a deformable A316 steel cylindrical vessel of 200 mm diameter. The shield base was welded to a flange, clamped by bolts to the diagrid,
- The above core structure (ACS) was a 1 mm thick deformable A316 cylinder of 140 mm diameter and 210 mm height, completely filled with water to avoid buckling of the wall as a consequence of the deflection of the base (also 1 mm thickness). The ACS was securely clamped to the deformable roof by bolts. The welded corner between wall and base plate was stiffened to avoid rupture.

The explosive charge was supported at the base of the ACS.

The whole test was well instrumented [13] with:
- 7 pressure transducers fitted under the roof at different radii,
- 8 strain gauges placed on the upper and lower sides of the roof at three radial locations (centre, mid-radius and near the boundary),
- 5 strain gauges attached at three main locations on the vessel (upper part of the lateral wall, charge level and base) to obtain axial and hoop strains,
- 6 strain gauges placed on internal structures:

2 on the above core structure (bottom and wall),
2 on the radial shield (charge level and top),
1 under the diagrid center,
1 on the collar supporting the core support structure,
• 2 high speed cameras used to obtain displacements of the roof and the vessel (upper bulge and base),
• residual deformations were evaluated by measuring, before and after the firing, mesh sizes of the grid drawn on the different structures.

3. Numerical modeling of the test-facility

The MARA10 test-facility is composed of structures and fluids interacting with each other. The mock-up is surrounded by a flexible roof and a flexible vessel and contains internal structures: the core support structure fixed to the vessel by a collar, the diagrid, the radial shield and the above core structures. The structures are assumed to be thin enough to be represented by shells except the core support structure which is supposed rigid.

Owing to the symmetry of the mock-up, an axisymmetric representation was used for the numerical simulation. The figure 3 presents the mesh used for the simulation of the MARA10 test and the figure 4 shows the representation of the structures.

In case of a HCDA, the internal fluids are sodium, argon and a gas bubble. In the MARA10 test, these fluids are respectively replaced by water, air and an explosive charge. Water and air are initially at the atmospheric pressure whereas the explosive charge induces an initial pressure of 165 MPa in the bubble area.

CASTEM-PLEXUS [37] [38] [39] [40] is a general fast dynamics finite element code devoted to the analysis of problems involving fast transients. It can deal with fluids and structures with a possibility of coupling. A specific CDA constitutive law was implemented in the code in order to be able to represent precisely this kind of explosion [41].

The characteristics taken into the numerical model are:

• Water	: $\rho = 998.3$ kg/m^3	sound speed $C = 1550$ m/s	$p^{(0)} = 10^5$ Pa
• Air	: $\rho = 1.206$ kg/m^3	$\lambda = c_p/c_v = 1.4$	$p^{(0)} = 10^5$ Pa
• Explosive charge	: $\rho = 400$ kg/m^3	polytropic coef. $\eta = \lambda = 1.24$	$p^{(0)} = 1.646\,10^8$ Pa

In CASTEM-PLEXUS, the fluids and solid structures can be described with an Eulerian, Lagrangian or A.L.E. (Arbitrary Lagrange Euler) approach. In the model, all the structures are represented with the lagrangian description and the mesh follows the deformation of the structures. The water and the air are described with an ALE modeling: the fluid grid is updated according to the deformation of the neighbouring structures. The bubble zone is kept fixed. Indeed if the bubble grid was ALE, the mesh would deform very much because of the expansion of the bubble gas at a very high initial pressure and this large deformation would entail numerical difficulties to carry out the computation. Moreover, the fixed bubble grid is used as a reference for the updating of the ALE surrounding mesh.

Two kinds of fluid-structure coupling are available in the CASTEM-PLEXUS code. Their main differences lie in the definition of the local normal vector used to write the coupling relations between the freedom degrees of the fluid and the solid. The first fluid-structure coupling (FS2D instruction) requires the definition of coupling elements by the user and imposes to the fluid nodes to have the same displacements as the structure nodes. However, there is no automatic actualisation of the ALE grid for the elements other than the ones on the coupled lines.

The second coupling (FSA instruction) goes without coupling elements; the code considers directly the fluid and solid nodes in contact and writes relations allowing a possible tangential movement of the fluid in relation to the structure. The FSA coupling is well adapted to complex geometries but it often implies a user intervention to pilot the displacements of the fluid ALE grid.

The FSA coupling was adopted for the MARA10 test because the presence of the internal structures involves large local displacements of the fluid grid. In the previous CASTEM-PLEXUS computations [33], the FS2D coupling was used because the FSA coupling was developed later. However, in the current model, a FS2D coupling persists in a local area.

As the diagrid is merely put down on the core support structure and as both structures are not rigidly linked, the diagrid extremity is linked to the CSS by a swivel contact. Consequently, there are two different structure nodes at the same location (the one pertaining to the diagrid and the other to the CSS) whereas there is only one fluid node facing the two structure ones. This configuration cannot be processed by the FSA coupling. Therefore a FS2D coupling was settled down at the connection between the diagrid, the core support structure and the fluid between the radial shield and the CSS.

The boundary conditions are:
• No horizontal displacement of the fluid nodes on the symmetry axis,
• No horizontal displacement and no rotation of the structure nodes located on the symmetry axis (ACS, diagrid, vessel),
• Complete blocking of the node in the top corner at the junction between the vessel and the roof,
• No horizontal displacement of the core support structure,
• Vertical displacement of the core support structure and of the diagrid extremity in contact with the CSS equal to the vertical displacement of the point at the intersection between the collar and the vessel.

In order to help the code to calculate correctly the ALE mesh updating in the areas of high fluid speed or high pressure variations, the user has to define relations governing the local displacement of the mesh. Three governing lines were set up.

The first line imposes to the fluid nodes between the ACS bottom corner and the radial shield top to stay aligned between both structure nodes during the displacement of the structures. This relation prevents a large deformation of the ALE grid due to the huge flow of the fluid going out from the central zone. Besides, this line is used as a reference for the updating of the fluid in the central zone.

The second line imposes to the fluid nodes between the radial shield top and the vessel to stay aligned between both structure points. This relation also helps the management of the fluid zone located out of the radial shield and above the collar and the core support structure.

The last line manages the interface between the water zone and the air layer. This line imposes to the fluid nodes at the interface to remain aligned between the two structure nodes pertaining respectively to the vessel and the above core structure and at the same level than the fluid nodes.

4. Analysis of the computed results

In this part, we try to present a synthesis of the results computed with the current version of CASTEM-PLEXUS [42]. Initially, a bubble gas is located in the centre of the mock-up and an air layer lays just below the roof. The rest of the test-facility is filled with water. All the fluids are at rest. The water and the air are at the atmospheric pressure while the bubble gas pressure is 165 MPa.

Between 0 and 0.06 ms, the expansion of the bubble gas causes the propagation of a pressure wave from the centre of the test-facility. The gas expands spherically with a velocity of about 200 m/s. The pressure wave hits the radial shield at 0.04 ms, the centre of the diagrid and the base of the Above Core Structure at 0.06 ms. A stress of 450 MPa appears at mid-height of the radial shield.

From 0.06 to 0.1 ms, the pressure wave crosses the three structures (shield, diagrid and ACS base) constituting a geometric confinement of the central zone. It continues its propagation out of the central zone. At 0.1 ms, the pressure wave impacts laterally the Core Support Structure. The bubble gas starts expanding preferentially towards the free space between the ACS base and the radial shield top. The velocity in that direction is around 150 m/s.

The top of the radial shield, the diagrid centre and the ACS base starts moving away from 0.1 ms. The whole radial shield is submitted to stresses from 0.08 ms, as well as the base of the ACS. At 0.1 ms, the lateral wall of the ACS and the external part of the diagrid in contact with the shield and the Core Support Structure are also submitted to stresses. Until that time, all the structures have an elastic behaviour.

Until 0.16 ms, the progression of the pressure wave leads to the impact of the vessel bottom, first on the symmetry axis and then on a larger size of the vessel base. The bubble gas is still confined in the central zone. The water hurled by the shock wave impacts perpendicularly the vessel base under the diagrid with a speed of about 50 m/s. The water is also propelled spherically in the rest of the test-facility. The diagrid is entirely submitted to stresses at 0.16 ms. Plastic strains appear in the upper part of the radial shield.

From 0.16 to 0.22 ms, the pressure wave propagates along the vessel bottom, goes round the whole CSS and impacts the collar attaching the CSS to the vessel. A depressurised zone forms between the radial shield and the CSS. The pressure wave impacts the top of the ACS whereas the roof is spared thanks to the presence of the air layer. At 0.22 ms, we note a first pressure peak against the ACS top.

Due to the shock wave, the whole radial shield moves away, the ACS base buckles as well as a bulge starts forming in the ACS lateral wall and that the ACS top starts going up. The diagrid continues moving down and the vessel bottom starts going down. The stress level increases in the radial shield, the diagrid and the ACS base and lateral wall. The vessel bottom and the collar are also submitted to stresses. Two high stress spots appear at the intersection of the diagrid, the shield and the CSS, and at the junction of the collar and the vessel. Besides of the radial shield, plastic strains appear in the ACS base.

Between 0.22 and 0.5 ms, the pressure decreases in the whole fluid zone. A high pressure of about 10 MPa persists in the central part of the mock-up. A pressure of about 6-8 MPa is remaining in the closed areas (in the ACS, below the CSS) and in the vicinity of the bottom corner. The bubble gas stays confined in the central part. Because of the confinement due to the diagrid and the shield, the bubble gas moves preferentially upwards and along a diagonal to try to escape by the free space between the ACS base and the shield top. In that area, the bubble velocity reaches some 100 m/s.

The water is ejected from below the diagrid towards the vessel bottom and under the CSS. The water is also ejected from the periphery of the radial shield towards the vessel lateral wall. Because of the depressurisation and the emptying of the area at the external periphery of the radial shield and the diagrid, the water vaporises around the shield and under the diagrid. The water impacts the lower part of the vessel lateral wall and then rebounds towards the collar. The water in the upper part of the mock-up orients progressively upwards, thus compressing the air layer against the roof.

We observe the continuation of the going down of the vessel bottom, the diagrid and the radial shield. The buckling of the ACS base and ACS wall becomes more marked. The ACS top moves up, thus pulling up the nearer part of the roof. The lower part of the vessel wall starts moving away, forming the lower bulge. As the vessel in the bottom corner starts going down, the corner opens.

The stresses increase everywhere, except in the rigid CSS and at the edge of the roof owing to the air presence protecting the roof. At 0.5 ms, the stresses are maximum in the central structures (diagrid, shield, ACS base and wall) and in the ACS wall. The top of the radial shield reaches a maximum plasticity level of 13 % and a maximum radial displacement of 15 mm. Owing to the stress rise in the ACS wall, plasticity appears half-way up this lateral wall. The centre of the vessel bottom becomes plastic too. High stress local zones appear in the vessel near the bottom corner, at the thickness change of the vessel and at the top of the lower bulge.

Between 0.5 and 0.15 ms, the pressure decreases in the whole test-facility. The bubble gas stops moving downwards and laterally. All the motion is concentrated towards the free space between the ACS and the shield. The bubble gas starts expanding out of the central zone with velocities up to 80 m/s.

The water in the ACS is hurled against the ACS top. Therefore the emptying of the lower part of the ACS causes the vaporisation of the water just above the base. Several pressure peaks are recorded in the centre of the ACS top. Owing to the bubble gas thrust, the ACS base keeps on moving up. A maximum stress of 600 MPa and a plastic strain level of 5 % are recorded in the ACS base at about 1 ms. Because of the internal water thrust, the ACS lateral wall buckling increases: it reaches a maximum extension and a maximum radial displacement of 2.4 mm at 0.7 ms. Then the lateral buckling remains constant.

Below the diagrid and the CSS, the downward water velocity decreases. However the vessel bottom goes on moving down, what pulls down the whole set of the Below Core Structures (diagrid, shield, CSS, collar) and the bottom corner of the vessel. The stresses remain constant in the vessel bottom. However the plastic strains increase at the centre of the vessel bottom. The stresses decrease in the Below Core Structures what leads to the constant maintaining of the plastic strains.

In the external half-part of the mock-up, the water in the upper part is propelled up by the bubble gas going out from the central zone. This water motion pushes the air layer upwards against the roof and horizontally along the roof towards the top corner. The going up of the roof at mid-radius starts around 0.7 ms. Between 0.5 and 1.5 ms, the stresses increase progressively in the whole roof, from the centre to the edge. A maximum stress level of 300 MPa is reached at 1.5 ms in the whole roof.

Half-way up the mock-up, the water flows either upwards or downwards along the vessel lateral wall. These fluid flows pushing the wall radially, the lower bulge reaches a maximum extension of 3.8 mm at 1 ms. Simultaneously, the water vaporises near the radial shield because the water goes away from this zone. The water hitting the bottom corner bounces afterwards towards the collar. These water impacts cause a concentration of stresses of 1000 MPa in the corner and 600 MPa near the collar attachment. In that area, the vessel becomes plastic.

Between 1.5 and 3 ms, the bubble gas goes on coming out of the central zone with speeds up to 100 m/s. As the bubble gas is still oriented downwards, even if the flow is very slowed down, the diagrid vertical displacement reaches a maximum of 33 mm at 2.7 ms. For the same reason with the water flow under the diagrid, the vessel bottom reaches a maximum fall of 35 mm at 2.8 ms.

In the Above Core Structure, the water rebounds on the top and then changes direction. Consequently, on the one hand, the whole ACS stops going up and starts coming back. On the other hand, the lateral bulge persists because the up and down water flows impose an identical pressure against the lateral wall. The location of the stressed zones in the ACS changes according to the fluid flows. At 2 ms, the ACS base reaches a maximum vertical displacement of 35 mm before going back.

The water in the bottom corner starts moving up what relieves the stresses in the corner. Nevertheless a maximum plastic strain of 7 % is reached at 3 ms. In the upper part, the water continues to push the air in the top corner. Owing to the small water flow along the ACS, the water vaporises near the ACS lateral wall. In the rest of the mock-up, the fluid flows are identical but slightly weaker. Globally, the stresses decrease in the structures except in the ACS.

From 3 to 9 ms, we observe the formation of a whirlpool against the ACS lateral wall and the radial shield top. After a phase of pulling out of the bubble gas from the central zone, the whirlpool pushes back the gas and water inside the central zone. Because of the whirlpool attracting water from the roof, the outer downward water flow balances partially the inner thrust of the ACS water flows, so that the ACS lateral wall moves back.

Because of the whirlpool too, the steam along the radial shield condenses. A last steam zone stays in the corner between the shield and the CSS. Below the diagrid, the water moves first up and then down. Consequently, the vessel bottom starts going back and finally moves down again.

Inside the ACS, the water alternates up and down flows according to the rebounds on the top and bottom surfaces of the ACS. Therefore the ACS base buckling changes its bending direction. As the water and air below the roof and in the top corner are pulled by the whirlpool, large fluid flows happen along the upper part of the vessel wall and an upper bulge creates from 3 ms. The air layer begins expanding from the top corner to its initial location and along the ACS wall.

5. Comparison with the experimental results and with previous numerical results

The purpose of our computations consists in qualifying the CASTEM-PLEXUS code for the computation of Core Disruptive Accidents and to estimate the progress realised in the modeling of the accident. Thus the current numerical results are compared with the experimental results and previous numerical results computed with the codes SIRIUS [13] and CASTEM-PLEXUS [33].

The comparison concerns:
- the vertical displacement of the vessel base,
- the hoop strain and the distance to the roof of the vessel upper bulge,
- the hoop strain of the vessel lower bulge,
- the vertical displacement of the roof (at the centre and at mid-radius),
- the vertical displacement of the diagrid,
- the hoop strain of the radial shield,
- the hoop strain of the lateral bulge of the ACS,
- the vertical strain of the ACS lateral wall,
- the impact pressure and the instant of maximum on the roof.

The figures 17 to 21 present respectively the vertical displacements of the vessel base, of the roof (at the centre of the ACS top and at mid-radius of the roof), of the diagrid, of the ACS base and of the extremities of the ACS lateral wall for the current CASTEM-PLEXUS computations. The figures 22 to 25 show respectively the maximum radial displacements of the upper bulge and lower bulge of the vessel lateral wall, of the radial shield top and of the ACS lateral wall for the current computations.

The figures 26 to 28 display respectively the pressure for the current CASTEM-PLEXUS computations, for the MARA10 experiment and the one obtained in the previous CASTEM-PLEXUS calculations. The results are collected in the table 1. The CASTEM-PLEXUS computations are noted CP in that table. The difference between the old and new CASTEM-PLEXUS computations comes from the treatment of the fluid-structure coupling.

The table 1 shows that, concerning the comparison of the computed vertical displacements of the vessel bottom with the experimental displacement, the new CASTEM-PLEXUS results are better (with 8 % error for the maximum displacement and 11 % for the final displacement) than the old CASTEM-PLEXUS results (respectively 24 % and 22 % error), themselves better than the SIRIUS results (42 % and 37 % error).

Regarding the maximum hoop strain of the lower bulge of the vessel, the new CASTEM-PLEXUS results are in the same order of magnitude as the SIRIUS ones. Even if they are slightly better, they still present a gap superior to 30 % compared with the strain measured in the MARA10 test. This information is not available for the old CASTEM-PLEXUS computations.

For the upper bulge of the vessel, the new computed hoop strain fits well with the experimental result (less than 7 % difference). This result is much better than the one computed previously by CASTEM-PLEXUS (around 150 % error) and a little better than the SIRIUS one (around 11 % gap). Concerning the distance to the roof, the new results once again fits very well with the experimental ones (3 % error, compared with 11 % error for SIRIUS and 88 % error for the old CASTEM-PLEXUS simulation).

The new CASTEM-PLEXUS simulation is less precise than the old one regarding the maximum vertical displacements of the roof (16 % error at the centre and 15 % at mid-radius, compared to 13 % error for the first one and the exact value for the second one). However, if one considers the final displacements, the new simulation is better than the old one (10 % error at the centre and exact value at mid-radius, compared to 26 % and 28 % differences). The SIRIUS results are much more unprecise than the ones issued from CASTEM-PLEXUS.

CASTEM-PLEXUS finds the right vertical displacement for the diagrid. The new results are better than the old ones themselves better than the SIRIUS ones. On the contrary, the SIRIUS results were much nearer than both CASTEM-PLEXUS ones about the hoop strain of the radial shield. Indeed, in the old CASTEM-PLEXUS simulation, the computed strain was twice the experimental value and the new simulation increases the discrepancy.

Concerning the lateral bulge of the Above Core Structure, the new hoop strain is almost half the experimental value. Even if this result has more or less the same magnitude as the SIRIUS result, the new CASTEM-PLEXUS computation is worse than the old one.

About the vertical crushing of the ACS lateral wall, the new CASTEM-PLEXUS results are in agreement with the SIRIUS ones; both fit well with the experimental results (about 10 % error). The new CASTEM-PLEXUS simulation improves seriously the precision of the result.

The last comparison concerns the pressure under the roof. The maximum pressure is observed at the centre of the ACS top. The shape of the pressure curve computed by CASTEM-PLEXUS in the new simulation is in agreement with the one of the MARA10 test. Indeed, CASTEM-PLEXUS finds a first peak of 18 MPa at 0.25 ms (instead of 25 MPa at 0.5 ms), then a succession of small peaks until 2.5 ms and later a second peak of 5.2 MPa at 6 ms (instead of 9 MPa at 5 ms). The new simulation is better than the old CASTEM-PLEXUS one because the timing of the first peak was not correct.

Generally, the new CASTEM-PLEXUS simulation is in a good agreement with the experimental results, except for the computation of the radial shield hoop strain. Moreover the new simulation is much better than the old one, what points out that the treatment of the fluid-structure coupling can influence seriously the results.

Whereas the SIRIUS code prediction was often better or comparable to the one of CASTEM-PLEXUS for the MARA8 test without internal structures, the SIRIUS prediction is much more unprecise than both CASTEM-PLEXUS ones in the case of the MARA10 test with the internal structures. This remark confirms the previous conclusion about the importance of a correct fluid-structure coupling as the fluid-structure coupling of SIRIUS was very simple, compared at once to the one of the old and new CASTEM-PLEXUS models.

6. Conclusion

In that paper, we present a computation of a Hypothetical Core Disruptive Accident in the MARA10 test-facility representing a simplified geometry of a reactor. This mock-up contains the main internal structures of the reactor block of a Liquid Metal Fast Breeder Reactor. The fluids intervening in the real accident were replaced by water, air and an explosive charge in the experiment.

In the numerical model, the structures are represented by shells. The internal fluids are described by the specific CDA constitutive law implemented on purpose in the CASTEM-PLEXUS code for computing this kind of explosion. The CASTEM-PLEXUS code succeeded in carrying out the computation of the explosion until 9 ms of physical time.

The explosive charge in the centre causes the propagation of a pressure wave which impacts first the radial shield, the diagrid and the Above Core Structure base and later the vessel bottom and vessel lateral wall and finally the roof.

The bubble gas expands in the central zone confined by the internal structures and afterwards it escapes in the rest of the mock-up by the narrow space between the ACS and the shield. Water vaporises out of the radial shield, below the diagrid and in the ACS. The air layer is compressed under the roof by the water pushed upwards by the explosion.

Very soon, the diagrid moves down, the radial shield goes away and the ACS base goes up. Then the vessel base moves down and the lateral wall goes away, thus creating a lower bulge. The ACS lateral wall buckles, the ACS top goes up, thus pulling up the rest of the roof. Finally, an upper bulge creates in the upper part of the vessel lateral wall and the ACS base changes curvature.

A comparison of the computed results was performed with the experimental results, as well as previous results issued from the codes SIRIUS and CASTEM-PLEXUS. The main difference between both CASTEM-PLEXUS models lays in the treatment of the fluid-structure coupling. The results showed that the current model is in a good agreement with the MARA10 results, apart from the simulation of the deflection of the radial shield.

Compared to the old numerical models, we notice a large improvement of the precision of the results. The new simulation is better than the old CASTEM-PLEXUS simulation, itself better than the simulation with the code SIRIUS. This test shows that a good treatment of the fluid-structure coupling is very important when internal structures are present inside the compartment.

For the last test of the MARA series (MARS test), specific developments for testing the influence of the internal structures were realised in the CASTEM-PLEXUS code. This mock-up contains, besides a more precise description of the internal structures present in the MARA10 test, a set of structures representing the heat exchangers and the pumps. These structures have a too complex geometry to mesh them. Consequently, a model was developed to homogenize the structures with the surrounding fluid [43] [44] and to take into account their presence simply.

References

[1] West, P.H., Hoskin, N.E. APRICOT - Phase 3. Suggested simple test problems for examination of thin shell modelling and fluid structure coupling, Aldermaston report AWRE/44/92/16, 1980. [2] Cagliostro, D.J., Florence, A.L., Abrahamson, G.R., 1979. Scale modeling in LMFBR safety, Nuclear Engineering and Design 55, 235-247.

[3] Kendall, K.C., Adnams, D.J., 1986. Experiments to validate structural dynamics code used in fast reactor safety assessment, Science and Technology of Fast Reactor Safety, Vol. 2, British Nuclear Energy Society, London, England.

[4] Holtbecker, H., 1977. Testing philosophy and simulation techniques, Nuclear Engineering and Design 42, 75-87.

[5] Hoskin, N.E., Lancefield, M.J., 1978. The COVA programme for the validation of computer codes for fast reactor containment studies, Nuclear Engineering and Design 46, 17-46.

[6] Albertini, C., et al. The JRC-COVA programme: Final Report. Commission of the European Communities, Report EUR 8705, 1983. Nuclear Science and Technology, 1984, pp. 1-182.

[7] Wenger, H.U., Smith, B.L., 1987. On the origin of the discrepancies between theory and experiment in the COVA series, Proc. 9th Int. Conf. on Structural Mechanics In Reactor Technology, Vol. E, Lausanne, Switzerland, pp. 339-344.

[8] Kendall, K.C., Benuzzi, A., 1980. The COVA programme : Validation of the fast reactor containment code SEURBNUK, Nuclear Engineering and Design 57, 79-105.

[9] Sidoli, J.E.A., Kendall, K.C. The WINCON programme - Validation of the fast reactor primary containment codes. Proc. INE Int. Conf. On Nuclear Containment, Cambridge, England, April 1987. Nuclear Containment Structures, D.G. Walton, Cambridge University Press, 1988.

[10] Acker, D., Benuzzi, A., Yerkess, A., Louvet, J., August 1981. MARA 01/02 - Experimental validation of the SEURBNUK and SIRIUS containment codes, Proc. 6th Int. Conf. on Structural Mechanics In Reactor Technology, Section E 3/6, Paris, France.

[11] Smith, B.L., Fiche, C., Louvet, J., Zucchini, A., August 1985. A code comparison exercise based on the LMFBR containment experiment MARA-04. Proc. 8th Int. Conf. on Structural Mechanics In Reactor Technology, Section E 4/7, Brussels, Belgium, pp. 151-157.

[12] Fiche, C., Louvet, J., Smith, B.L., Zucchini, A., August 1985. Theoretical experimental study of flexible roof effects in an HCDA's simulation, Proc. 8th Int. Conf. on Structural Integrity In Reactor Technology, Section E 4/5, Brussels, Belgium, pp. 139-144.

[13] Louvet, J., Hamon, P., Smith, B.L., Zucchini, A., August 1987. MARA 10: an integral model experiment in support of LMFBR containment analysis, Proc. 9th Int. Conf. on Structural Mechanics In Reactor Integrity, Section E, Lausanne, Switzerland, pp. 331-337.

[14] Falgayrettes, M., Fiche, C., Granet, P., Hamon, P., Barrau, P., Magnon, B., Jalouneix, J., Nédélec, M., 1983. Response of a 1/20 scale mock-up of the Superphenix breeder reactor to an HCDA loading simulation, Proc. 7th Int. Conf. on Structural Mechanics In Reactor Technology, Section E 4/1, Chicago, USA, pp. 157-166.

[15] Cowler, M.S., Hancock, S.L., 1979. Dynamic fluid-structure analysis of shells using the PISCES 2 DELK computer code, Proc. 5th Int. Conf. on Structural Mechanics In Reactor Technology, Section B 1/6, Berlin, Germany.

[16] Chang, Y.W., Gvildys, J., Fistedis, S.H., 1974. Analysis of the primary containment response using a hydrodynamic-elastic-plastic computer code, Nuclear Engineering and Design 27, 155-175.

[17] Chang, Y.W., 1977. Application of containment codes to LMFBRs in the United States, Nuclear Engineering and Design 42, 53-67.

[18] Stiévenart, M., Bouffioux, P., Eglème, M., Fabry, J.P., Lamotte, H. August 1975. Analysis of LMFBR explosion model experiments by means of the Surboum-II code, Proc. 3rd Int. Conf. on Structural Mechanics In Reactor Technology, Section E 3/5, London, England.

[19] Cameron, I.G., Hankin, B.C., Warham, A.G.P., Benuzzi, A., Yerkess, A., August 1977. The computer code SEURBNUK-2 for fast reactor explosion containment safety studies, Proc. 4th Int. Conf. on Structural Mechanics In Reactor Technology, Section B 2/1, San Francisco, USA.

[20] Smith, B.L., Yerkess, A., Adamson, J., August 1983. Status of coupled fluid-structure dynamics code SEURBNUK, Proc. 7th Int. Conf. on Structural Mechanics In Reactor Technology, Section B 9/1, Chicago, USA.

[21] Smith, B.L., Yerkess, A., Washby, V., August 1987. The computer code SEURBNUK-EURDYN: First release version, Proc. 9th Int. Conf. on Structural Mechanics In Reactor Technology, Lausanne, Switzerland.

[22] Cigarini, M., Daneri, A., Toselli, G., August 1983. Applications of ASTARTE-4 code to explosive models with complex internal structure using the rezoning facility, Proc. 7th Int. Conf. on Structural Mechanics In Reactor Technology, Section B 9/3, Chicago, USA.

[23] Graveleau, J.L., Louvet, P., August 1979. Calculation of fluid-structure interaction for reactor safety with the CASSIOPEE code, Proc. 5th Int. Conf. on Structural Mechanics In Reactor Technology, Section B 1/7, Berlin, Germany.

[24] Blanchet, Y., Obry, P., Louvet, J., August 1981. Treatment of fluid-structure interaction with the SIRIUS computer code, Proc. 6th Int. Conf. on Structural Mechanics In Reactor Technology, Section B 8/8, Paris, France.

[25] Daneri, A., Toselli, G., Trombetti, T., Blanchet, Y., Louvet, J., Obry, P., August 1981. Influence of the representation models of the stress-strain law on the LMFBR structures in an HCDA, Proc. 6th Int. Conf. on Structural Integrity In Reactor Technology, Section E 4/4, Paris, France.

[26] Louvet., J., August 1989. Containment response to a core energy release. Main experimental and theorical issues - Future trends, Proc. 10th Int. Conf. on Structural Mechanics In Reactor Integrity, Vol. E, Anaheim, pp. 305-310.

[27] Bour, C., Spérandio, M., Louvet, J., Rieg, C., August 1989. LMFBR's core disruptive accident. Mechanical study of the reactor block, Proc. 10th Int. Conf. on Structural Mechanics In Reactor Technology, Vol. E, Anaheim, pp. 281-287.

[28] Lepareux, M., Bung, H., Combescure, A., Aguilar, J., August 1991. Analysis of a CDA in a LMFBR with a multiphasic and multicomponent behaviour law, Proc. 11th Int. Conf. on Structural Mechanics In Reactor Integrity, Section E 13/1, Tokyo, Japan, pp. 371-376.

[29] Casadei, F., Daneri, A., Toselli, G., August 1989. Use of PLEXUS as a LMFBR primary containment code for the CONT benchmark problem, Proc. 10th Int. Conf. on Structural Mechanics In Reactor Technology, Section E 13/1, Anaheim, pp. 299-304.

[30] Benuzzi, A., 1987. Comparison of different LMFBR primary containment codes applied to a benchmark problem, Nuclear Engineering and Design 100, 239-249.

[31] Lepareux, M., Bung, H., Combescure, A., Aguilar, J., Flobert, J.F., August 1993. Analysis of an HCDA in a fast reactor with a multiphase and multicomponent behavior law, Proc. 12th Int. Conf. on Structural Mechanics In Reactor Integrity, Section E 7/2, Stuttgart, Germany, pp. 197-202.

[32] Cariou[a], Y., Pirus, J.P., Avallet, C., August 1997. LMR large accident analysis method, Proc. 14th Int. Conf. on Structural Mechanics In Reactor Technology, Section P 3/7, Lyon, France, pp. 395-402.

[33] Cariou, Y., Spérandio, M., Lepareux, M., Christodoulou, K., August 1993. LMFBR's whole core accident. Validation of the PLEXUS code by comparison with MARA tests, Proc. 12th Int. Conf. on Structural Mechanics In Reactor Technology, Section E 7/4, Stuttgart, Germany.

[34] Cariou[b], Y., Lepareux, M., Noé, H., August 1997. LMR's whole core accident. Validation of the PLEXUS code by comparison with MARS test, Proc. 14th Int. Conf. on Structural Mechanics In Reactor Technology, Section P 2/6, Lyon, France, pp. 339-346.

[35] NERSA, 1987. The Creys-Malville power plant, Electricité de France, Direction de l'équipement, Région d'équipement Alpes-Lyon, France.

[36] David, F., 1978. Etude d'une composition explosive flegmatisée. Applications à la déformation d'une cuve, Proc. Symposium sur les hautes pressions dynamiques, Paris, France.

[37] Chavant, C., Hoffmann, A., Verpeaux, P., Dubois, J., 1979. Plexus: A general computer code for explicit Lagrangian computation, Proc. 5th Int. Conf. on Structural Integrity In Reactor Technology, Section B 2/8, Berlin, Germany.

[38] Hoffmann, A., Lepareux, M., Schwab, B., Bung, H., 1984. Plexus - A general computer program for fast dynamic analysis, Proc. Conference on Structural Analysis and Design on Nuclear Power Plant, Porto Alegre, Brazil.

[39] Robbe, M.F., Lepareux, M., Bung, H. Plexus - Notice théorique, CEA report DMT/94-490, 1994.

[40] Robbe[a], M.F., Galon, P., Yuritzinn, T., November 1999. Castem-Plexus: Un logiciel de dynamique rapide pour évaluer l'intégrité des structures en cas d'accident, Proc. 4th Conf. INSTRUC, Courbevoie, France.

[41] Robbe[a], M.F., Cariou, Y., Lepareux, M., Treille, E., September 2000. Numerical simulation of a Hypothetical Core Disruptive Accident in the MARA8 mock-up with the CASTEM-PLEXUS computer code, Proc. European Congress on Computational Methods in Applied Sciences and Engineering (ECCOMAS), Barcelona, Spain.

[42] Robbe[b], M.F., Cariou, Y., Lepareux, M., Treille, E., September 2000. Numerical interpretation of the MARA10 test simulating a Hypothetical Core Disruptive Accident in a mock-up schematizing a reactor, Proc. European Congress on Computational Methods in Applied Sciences and Engineering (ECCOMAS), Barcelona, Spain.

[43] Robbe[b], M.F., August 1999. A porosity method to model the internal structures of a reactor vessel, Proc. 15th Int. Conf. on Structural Mechanics In Reactor Technology, Vol. B, Seoul, Korea.

[44] Robbe[c], M.F., Bliard, F., April 1999. A porosity model to represent the influence of structures on a fluid flow. Application to a hypothetical core disruptive accident, Proc. 7th Int. Conf. On Nuclear Engineering, paper 7819, Tokyo, Japan.

		Experiment		SIRIUS computations		Old CP computations		New CP computations	
		Maximum	Final	Maximum	Final	Maximum	Final	Maximum	Final
Vessel bottom	Vert. displacement (cm)	3.8	2.7	2.2	1.7	2.9	2.1	3.5	3.0
Vessel lower bulge	Hoop strain (%)	1.7	1.3	1.0	0.8			1.1	0.9
Vessel upper bulge	Hoop strain (%)	2.9	2.7	2.6	2.4	7.1	6.8	2.7	2.5
	Distance to the roof (cm)		6.3		5.6		11.9		6.1
Roof	Vert. displacement at the centre (cm)	3.1	1.9	2.2	1.8	2.7	2.4	2.6	2.1
	Vert. displacement at mid-radius (cm)	2.0	1.4	1.5	1.2	2.0	1.8	1.7	1.4
Diagrid	Vert. displacement at the centre (cm)		3.1	2.7	1.9	4.1	2.9	3.3	3.0
Radial shield	Hoop strain (%)	6.0	4.2	6.2	6.0	13.3	12.2	15	12
Lateral wall of the ACS	Hoop strain of the bulge (%)		6.4		3.4		4.1	3.4	3.3
	Vertical strain of the wall (%)		-2.6		-2.4		-1.1		-2.4
		1^{st} impact	2^{nd} impact	1^{st} impact	2^{nd} impact	1^{st} impact	2^{nd} impact	1^{st} impact	2^{nd} impact
Pressure under the roof	Max. pressure (MPa)	25	9			16	6	centre: 18 else: 8	centre: 5.2 else: 7
	Instant of max (ms)	0.5	5.0			2.8	4.2	0.25	4 to 6

Table 1: Comparison between the experimental results and the results computed by SIRIUS and CASTEM-PLEXUS

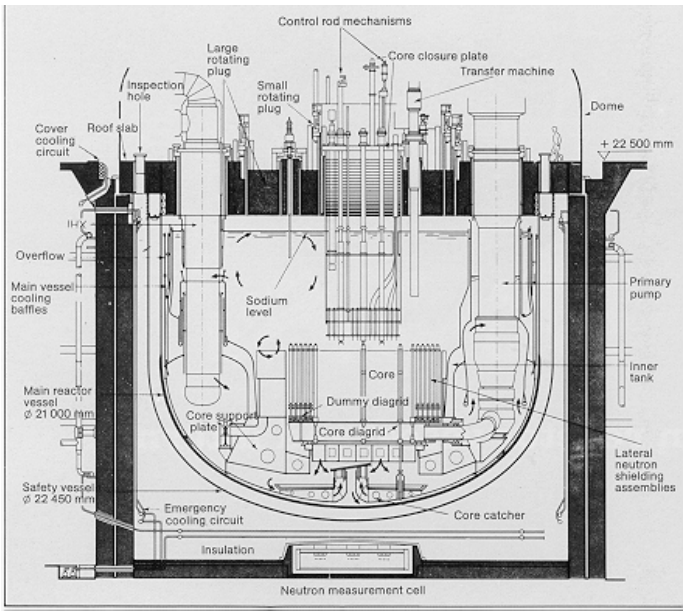

Fig. 1: The Superphenix reactor

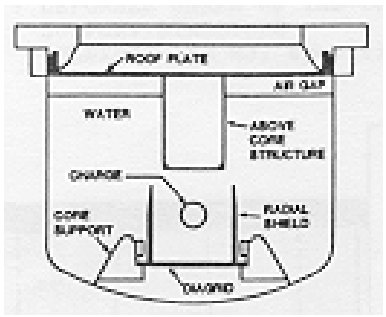

Fig. 2: The MARA10 test-facility

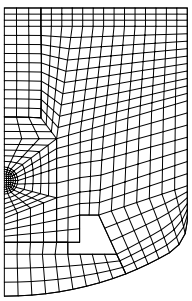

Fig. 3: Mesh of the MARA10 test

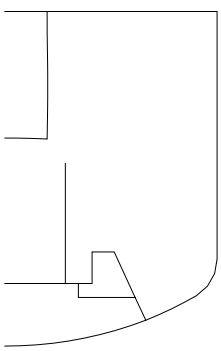

Fig. 4: Mesh of the structures

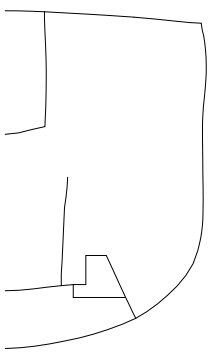

Fig. 12: Deformed shape of the structures at 9 ms

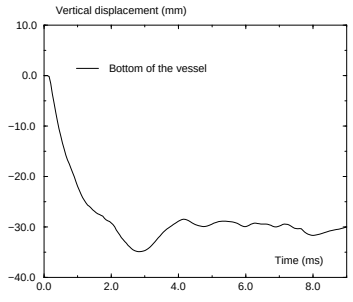

Fig. 17: Vertical displacement of the vessel bottom

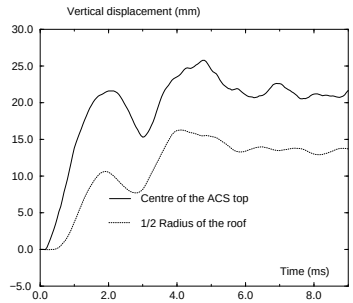

Fig. 18: Vertical displacement of the roof

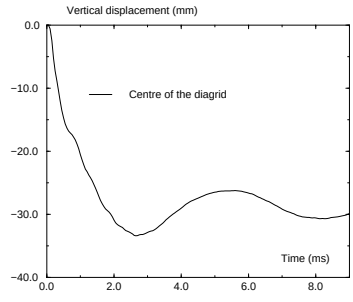

Fig. 19: Vertical displacement of the diagrid

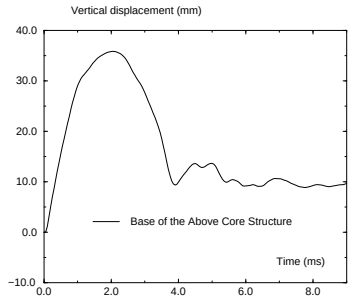

Fig. 20: Vertical displacement of the base of the Above Core Structure

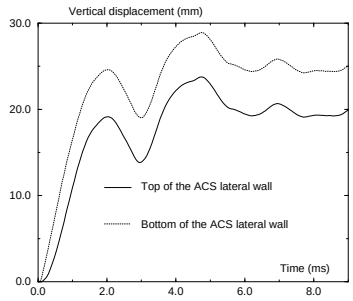

Fig. 21: Vertical displacement of the extreme points of the ACS lateral wall

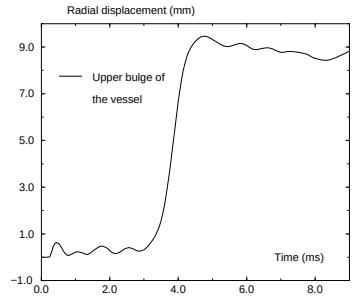

Fig. 22: Radial displacement of the upper bulge on the vessel lateral wall

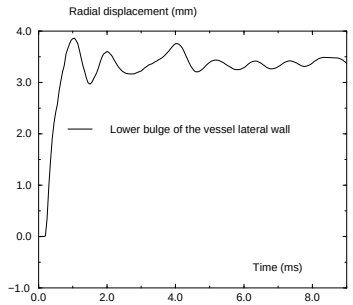

Fig. 23: Radial displacement of the lower bulge on the vessel lateral wall

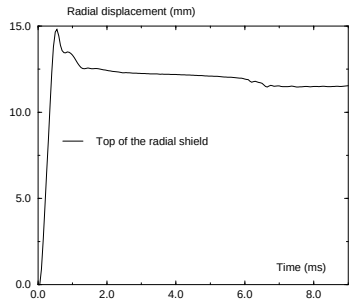

Fig. 24: Radial displacement of the radial shield

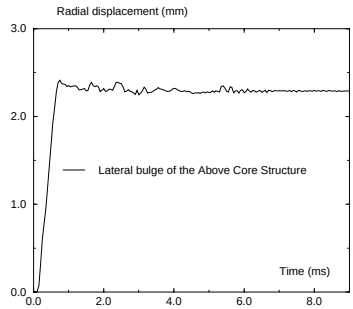

Fig. 25: Radial displacement of the lateral wall of the Above Core Structure

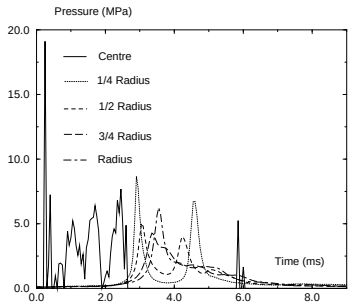

Fig. 26: Pressure under the roof

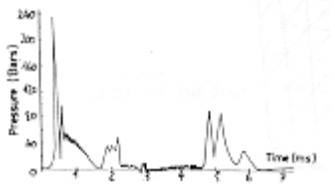

Fig. 27: Experimental pressure

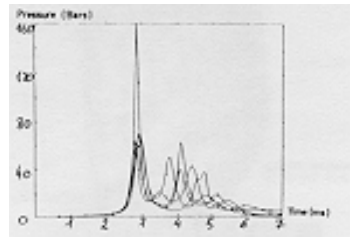

Fig. 28: Pressure under the roof, computed previously